

## UNVEILING THE IMPORTANT ROLE OF GROUPS IN THE EVOLUTION OF MASSIVE GALAXIES: INSIGHTS FROM AN INFRARED PASSIVE SEQUENCE AT INTERMEDIATE REDSHIFT

D. J. WILMAN,<sup>1</sup> D. PIERINI,<sup>1</sup> K. TYLER,<sup>2</sup> S. L. MCGEE,<sup>3</sup> A. OEMLER, JR.,<sup>4</sup>  
S. L. MORRIS,<sup>5</sup> M. L. BALOGH,<sup>3</sup> R. G. BOWER,<sup>5</sup> AND J. S. MULCHAEY<sup>4</sup>

Received 2007 October 23; accepted 2008 February 12

### ABSTRACT

The most massive galaxies in the universe are also the oldest. To overturn this apparent contradiction with hierarchical growth models we focus on the group-scale halos that host most of these galaxies. Our  $z \sim 0.4$  group sample is selected in redshift space from the CNOC2 redshift survey. A stellar mass–selected  $M_* \gtrsim 2 \times 10^{10} M_\odot$  sample is constructed using IRAC observations. A sensitive mid-infrared (MIR) IRAC color is used to isolate passive galaxies. It produces a bimodal distribution, in which passive galaxies (highlighted by morphological early types) define a tight MIR color sequence (infrared passive sequence, IPS). This is due to stellar atmospheric emission from old stellar populations. Significantly offset from the IPS are galaxies where reemission by dust boosts emission at  $\lambda_{\text{obs}} = 8 \mu\text{m}$ . We term them infrared excess galaxies, whether star formation and/or AGN activity are present. They include all known morphological late types. Comparison with EW[O II] shows that MIR color is highly sensitive to low levels of activity and allows us to separate dusty active from passive galaxies at high stellar mass. The fraction of infrared excess galaxies,  $f(\text{IRE})$ , drops with  $M_*$ , such that  $f(\text{IRE}) = 0.5$  at a “crossover mass” of  $M_{\text{cr}} \sim 1.3 \times 10^{11} M_\odot$ . Within our optically defined group sample there is a strong and consistent deficit in  $f(\text{IRE})$  at all masses, but most clearly at  $M_* \gtrsim 10^{11} M_\odot$ . Suppression of star formation must mainly occur in groups. In particular, the observed trend of  $f(\text{IRE})$  with  $M_*$  can be explained if suppression of  $M_* \gtrsim 10^{11} M_\odot$  galaxies occurs primarily in the group environment. This is confirmed using a mock galaxy catalog derived from the millenium simulation. In this way, the mass-dependent evolution in  $f(\text{IRE})$  (*downsizing*) can be driven solely by structure growth in the universe, as more galaxies are accreted into group-sized halos with cosmic time.

*Subject headings:* galaxies: clusters: general — galaxies: evolution — galaxies: high-redshift —  
galaxies: photometry — galaxies: statistics — infrared: galaxies

### 1. INTRODUCTION

Perhaps the biggest puzzle of galaxy formation in recent decades has been the early and rapid formation of the most massive galaxies (Bender et al. 1998; Cimatti et al. 2004). This apparently supported the “monolithic collapse” model (Eggen et al. 1962), in contradiction to the standard picture of a cold dark matter (CDM) universe, in which galaxies grow hierarchically through mergers, along with the dark matter halos in which they are embedded (e.g., Benson et al. 2002). Observationally, the picture has been embellished by recent galaxy surveys from  $z \sim 0$  to  $\sim 1.5$ . Going to higher galaxy mass and to denser environments, galaxies are older (Kauffmann et al. 2003; Panter et al. 2003; Poggianti et al. 2004; Thomas et al. 2005; Salim et al. 2005) and more likely to have experienced a shorter star-forming life, which is now truncated (Yamada et al. 2005; Baldry et al. 2006; Pannella et al. 2006; Haines et al. 2008; Bundy et al. 2006; Hopkins et al. 2007). The term *downsizing* (Cowie et al. 1999) is used to describe the earlier and less extended star formation histories in more massive galaxies.

Recent attempts to explain downsizing trends have examined the ways in which gas heating and cooling depend on mass and

redshift (e.g., Dekel & Birnboim 2006) and invoked new heating methods such as feedback from active galactic nuclei (AGNs; Bower et al. 2006; Croton et al. 2006). Regardless of the physics, a hierarchical universe can itself supply a natural explanation for dependence of galaxy properties on stellar mass and on environment at the same time (De Lucia et al. 2006). As more and more massive galaxies are incorporated into more and more massive halos, the probability of star formation being truncated is increased. Even in the populous loose group environment the properties of galaxies depend strongly on environment (e.g., Postman & Geller 1984; Zabludoff & Mulchaey 1998; Lewis et al. 2002; Gómez et al. 2003; Balogh et al. 2004; Wilman et al. 2005; Weinmann et al. 2006; Gerke et al. 2007). Thus, evolution in groups can play an important role in driving evolutionary trends.

The fraction of passive galaxies increases steadily and monotonically with increasing stellar mass. It is therefore convenient to quantify downsizing trends by identifying a stellar mass at which the fraction of passive (or red/early-type) galaxies is defined to be exactly 50%. This has no physical significance, so we prefer to call this the “crossover mass” ( $M_{\text{cr}}$ ) rather than the “transition mass” (e.g., Bundy et al. 2006). The variable  $M_{\text{cr}}$  decreases strongly with increasing environmental density (Baldry et al. 2006; Bundy et al. 2006; Haines et al. 2008), with a maximum  $M_{\text{cr}} \sim 2 \times 10^{10} M_\odot$  in the *lowest density environments*, where the  $z \sim 0$  red galaxy fraction is 50% (Baldry et al. 2006). The evolution of  $M_{\text{cr}}$  for the global population indicates  $M_{\text{cr}} \sim (2.5\text{--}6) \times 10^{10} M_\odot$  at  $z \sim 0.4$  and  $M_{\text{cr}} \sim (7\text{--}10) \times 10^{10} M_\odot$  at  $z \sim 1$  (Hopkins et al. 2007).

These studies, mostly at rest-frame UV-to-optical wavelengths, are hindered by the strong correlation between galaxy mass and dust attenuation in star-forming galaxies (Giovannelli et al. 1995;

<sup>1</sup> Max-Planck-Institut für extraterrestrische Physik, Giessenbachstraße, D-85748 Garching, Germany.

<sup>2</sup> Steward Observatory, University of Arizona, 933 North Cherry Avenue, Tucson, AZ 85721.

<sup>3</sup> Department of Physics and Astronomy, University of Waterloo, Waterloo, ON N2L 3G1, Canada.

<sup>4</sup> Observatories of the Carnegie Institution, 813 Santa Barbara Street, Pasadena, CA.

<sup>5</sup> Physics Department, University of Durham, South Road, Durham DH1 3LE, UK.

Wang & Heckman 1996; Masters et al. 2003; Brinchmann et al. 2004; Weiner et al. 2007). This correlation may arise directly from the variations of star formation history with mass (Calura et al. 2008) and can lead to confusion between truly passive and dusty star-forming galaxies. In some cases light from the youngest stars can be totally removed from the line of sight, not only because their SED peaks at shorter wavelengths where dust attenuation is most effective (e.g., Pierini et al. 2004), but also because the H II regions in which they are embedded can be particularly dusty (Duc et al. 2002; Tuffs et al. 2004). This degeneracy of passive versus dusty star-forming galaxies is well known at high redshifts, where a selection of optically red galaxies (extremely red object/galaxy, ERO/ERG, or distant red galaxy, DRG) is more and more likely to select dusty starbursts as one moves to even higher redshift (from  $\sim 50\%$  at  $z \sim 1$  [Cimatti et al. 2002; Lotz et al. 2008] to  $\geq 90\%$  at  $z \sim 2-3$  [Papovich et al. 2006], with an increasing contribution from increasingly active infrared-bright galaxies [Caputi et al. 2006; Daddi et al. 2007]).

Even in the local universe the optical red sequence (e.g., Bower et al. 1992) is contaminated with star-forming galaxies and some AGNs. These “interlopers” can be identified using optical or UV color-color diagrams or high signal-to-noise ratio emission-line measurements (e.g., Wolf et al. 2005; Haines et al. 2008). However, the dust emission really stands out in the infrared, where the absorbed energy (mainly nonionizing UV photons) is re-emitted (Popescu et al. 2000 and references therein). Thirty-one percent of red sequence galaxies (by number density) are  $24 \mu\text{m}$  bright, corresponding to  $\sim 17\%$  star-forming galaxies and  $\sim 14\%$  AGN host galaxies (Davoodi et al. 2006).

At shorter wavelengths ( $\sim 3-12 \mu\text{m}$ ) strong emission features exist in the presence of star formation (Phillips et al. 1984; Roche et al. 1991). However, they are usually absent in the more highly ionized environments typical of AGNs (Aitken et al. 1982; Roche et al. 1984, 1991). These have been identified as PAH (polycyclic aromatic hydrocarbon) features (most obviously characterized by the strong, broad emission features at  $6.2, 7.7, 8.6,$  and  $11.3 \mu\text{m}$ ; Leger & Puget 1984; Desert et al. 1990) and loosely trace star formation rates on the scale of a galaxy (Roussel et al. 2001). Spectral diagnostics have been developed using the strengths of these features to distinguish star formation from nuclear activity (Genzel et al. 1998; Laurent et al. 2000). PAH carriers are apparently ubiquitous in high-metallicity star-forming galaxies (e.g., Boselli et al. 1998; Genzel & Cesarsky 2000; Draine et al. 2007), although in low-metallicity galaxies they may be absent (Engelbracht et al. 2005; Draine et al. 2007). Calibration of physical quantities, such as star formation rate, from PAH bands is complicated by the relative importance of circumstellar dust and diffuse dust heated by the general radiation field or collisional impacts. These components may be significant for galaxies with low to moderate star formation rates and dust contents (see, e.g., Boselli et al. 2004; Pérez-González et al. 2006; Calzetti et al. 2007).

To keep things simple, one can construct mid-infrared (MIR) colors as opposed to calibrating star formation rates. The wealth of information in this spectral range prompted the use of MIR colors to trace star formation, dust temperature, and nuclear activity (e.g., Dale et al. 2000; Boselli et al. 2003; Fisher 2006). Normalizing the flux from a dust-sensitive band ( $\lambda_{\text{rest}} \gtrsim 6 \mu\text{m}$ ) by a stellar mass-sensitive band (tracing old stellar populations, e.g., at  $3.6 \mu\text{m}$ ) produces a MIR color highly sensitive to the level of dust emission per unit stellar mass. This is especially well correlated with morphology, tracing the warm dust emission from star-forming spiral arms (Pahre et al. 2004a). Indeed, in the local universe the MIR color can effectively predict morphology. Li et al. (2007) find  $88\%$  early types below  $\nu L_{\nu}(8)/\nu L_{\nu}(3.6) = 0.303$

and  $83\%$  late types above this division.<sup>6</sup> The combined sample exhibits a bimodal distribution in MIR color. Johnson et al. (2007) also see this bimodality in MIR colors for galaxies in Hickson compact groups and show that the fraction of MIR-passive galaxies is much higher in the more evolved (H I-poor and X-ray-bright) groups. These results demonstrate the power of IRAC colors to separate truly passive galaxies from star-forming or AGN host galaxies without the dust-driven degeneracies of optical and UV studies.

Our goal is to isolate truly passive galaxies and thus trace the buildup of the increasingly important population of passively evolving galaxies in the universe as a function of environment. In particular, we wish to study massive ( $M_* \gtrsim 2 \times 10^{10} M_{\odot}$ ) galaxies at  $z \sim 0.4$ , where the contributions of both passive and dusty star-forming galaxies are important but can be confused with each other without due attention. Separating these populations using the MIR color will alleviate this problem. Strong evolution in the dust and star formation properties of normal galaxies over the range  $0 < z \lesssim 0.7$  is expected: at  $z \gtrsim 0.7$  spirals dominate the luminous infrared galaxy (LIRG) population (Bell et al. 2005; Rowan-Robinson et al. 2005; Zheng et al. 2007), while today galaxies of equivalent infrared luminosities are much rarer and are typically interacting systems and mergers. Our galaxy sample, selected from the CNOC2 redshift survey (Yee et al. 2000), probes intermediate redshifts ( $z \sim 0.4$ ). This redshift corresponds to a look-back time of  $\sim 3-4$  Gyr, when the volume-averaged star formation rate in the universe was significantly higher than it is today (Lilly et al. 1996; Madau et al. 1998; Hopkins 2004).

In § 2 our sample is introduced, including archive IRAC data in our fields. From this stellar masses and MIR colors are derived, and a mass-selected sample is constructed. Selection effects will be discussed in detail. Section 3 presents the MIR colors of  $z \sim 0.4$  galaxies as a function of their stellar masses and morphologies. A tight *infrared passive sequence* is identified in the MIR color-mass plane as a tool to select passive galaxies. Section 4 examines the correlation of MIR color with the EW[O II]  $\lambda 3727$  emission-line diagnostic, testing their relative sensitivity. In § 5 we compute the fraction of massive galaxies with infrared excess (IRE galaxies) as a function of stellar mass. The role of the group environment is discussed in § 6, where we examine galaxies in our optical group catalog (Carlberg et al. 2001). Finally, our results are discussed in the context of our current understanding of galaxy evolution and the group environment in § 7. In particular, by applying a simple model to a mock galaxy catalog, we focus on the possibility that downsizing is intimately related to, if not entirely caused by, the growth of structure with time. Our conclusions are presented in § 8. Throughout this paper a  $\Lambda$ CDM cosmology with  $\Omega_m = 0.3$ ,  $\Omega_{\Lambda} = 0.7$ , and  $H_0 = 100 h \text{ km s}^{-1} \text{ Mpc}^{-1}$ , where  $h = 0.75$ , is assumed.

## 2. SAMPLE

The objective of this paper is to study MIR activity in galaxies as a function of their stellar mass and environment. This is facilitated by the construction of a mass-selected sample in the redshift range  $0.3 \leq z \leq 0.48$ , described in this section.

### 2.1. CNOC2 Survey and Groups

Our sample is based on the CNOC2 redshift survey, which is magnitude limited down to  $R_C \sim 23.2$  in photometry and totals  $\sim 1.5$  square degrees within four separate patches on the sky. Spectroscopic redshifts exist for a large and unbiased sample of  $R_C \lesssim 21.5$  galaxies (Yee et al. 2000). Within the fields of

<sup>6</sup> Includes assumed stellar contribution to  $\nu L_{\nu}(8)$  of  $0.232\nu L_{\nu}(3.6)$ .

20 kinematically selected groups from the catalog of Carlberg et al. (2001) the original  $UBVR_C I_C$  photometry and spectroscopy have been supplemented with targeted spectroscopy to  $R_C = 22$  using the Magellan 6.5 m telescope (Wilman et al. 2005) and F775W-band *HST* ACS imaging. Galaxies with spectroscopic redshifts  $z > 0.3$  and ACS coverage have been visually morphologically classified by one of the authors (A. Oemler, Jr., hereafter AO).

The probability that a galaxy has a redshift is a function of its  $R_C$ -band magnitude and is unbiased to  $R_C = 21.5$ . To study the statistical properties of galaxies as a function of their stellar mass (and not  $R_C$ -band magnitude) we must statistically correct for this selection function and magnitude limit. This is achieved by weighting galaxies by the inverse probability that they appear in the  $R_C \leq 21.5$  spectroscopic sample. There are two components to this weight:

1. A weight  $W_{R_C}$  to account for the fraction of galaxies that are targeted spectroscopically (with measured redshifts) as a function of  $R_C$ -band magnitude. Since below  $R_C = 21.5$  the success of redshift determination may be biased in favor of emission-line galaxies,  $W_{R_C}$  is set to 0 for  $R_C > 21.5$ .

2. A weight  $W_z$  to account for the fraction of sample volume within which a galaxy would fall out of our  $R_C \leq 21.5$  sample (effectively a  $V_{\max}$  correction). For a  $0.3 \leq z \leq 0.48$  sample, this means that for each  $R_C \leq 21.5$  galaxy in the sample,  $W_z = V(z = 0.3-0.48)/V(z = 0.3 \text{ to } z_{\text{lim}})$ , where  $V$  is the cosmological volume in our chosen cosmology and  $z_{\text{lim}}$  is the redshift at which the galaxy would have a magnitude  $R_C = 21.5$ .

Then the final weight for each galaxy is simply:  $W = W_{R_C} W_z$ .

## 2.2. IRAC Photometry

The *Spitzer Space Telescope* GTO program 64 (PI G. G. Fazio) included an IRAC (Infrared Array Camera; Fazio et al. 2004) scan-map survey of  $\sim 20' \times 30'$  regions in the center of three of the four CNOC2 patches. The IRAC focal plane geometry translates each mapping into one mapping of bands 1 ( $3.6 \mu\text{m}$ ) and 3 ( $5.8 \mu\text{m}$ ) and another mapping of bands 2 ( $4.5 \mu\text{m}$ ) and 4 ( $8.0 \mu\text{m}$ ), offset by  $6.7'$ .

The astrometrically and photometrically calibrated post-BCD (post-basic calibrated data) products were retrieved from the *Spitzer* archive. The pipeline version used was S11.4.0. The processed images are clean, with no image artifacts, and provide stable source flux measurements and accurate subarcsecond astrometry. Apart from at the map edges, all sources receive  $\sim 500$  s imaging time in all four bands (100 s frame time at five dithered positions). The complete four-band IRAC coverage has significant ( $\geq 50\%$ ) overlap with six ACS fields, where galaxies have also been morphologically classified. Shallow MIPS  $24 \mu\text{m}$  imaging is also available, but with lower sensitivity and poorer diffraction-limited resolution than the IRAC bands.

For all sources detected in the  $3.6 \mu\text{m}$  frame, colors are measured using the SExtractor package (Bertin & Arnouts 1996) in double-image mode. They are derived from fluxes measured inside  $3''$  radius apertures centered at the position of all  $3.6 \mu\text{m}$ -detected objects, in all IRAC bands. Detection requires at least four adjacent pixels that are at least  $1.5 \sigma$  above the background level at  $3.6 \mu\text{m}$ . Aperture corrections were computed to correct for light lost from the aperture due to the spatial extent of the PRF (point-response function).<sup>7</sup> Corrected measurements are used to compute flux ratios (colors) within the aperture. The SExtractor

FLUX\_AUTO Kron-like measurement provides more stable total flux measurements and thus is used to compute absolute galaxy luminosity at  $3.6 \mu\text{m}$ . We follow the practice of SWIRE<sup>8</sup> and compute the flux error from the measurement image itself, weighted by inverse variance using the coverage map.

To match the  $3.6 \mu\text{m}$ -selected catalog to the CNOC2 redshift catalog, we apply the `tmatch` tool in IRAF.<sup>9</sup> None of the galaxies in our spectroscopic sample are lost from the IRAC sample due to lack of sensitivity except at the edge of the IRAC field. Visual inspection shows that CNOC2 galaxies with no match either lie outside the IRAC zone of full coverage, can be identified with sources improperly deblended by SExtractor, or lie in regions of particularly poor CNOC2 astrometry. The sample is then limited to those objects with unambiguous matches, with no apparent bias relative to the  $\sim 15\%$  of CNOC2 galaxies with IRAC coverage, which are lost at this stage. However, to maintain statistical accuracy the weight  $W_{R_C}$  is modified to account for galaxies without spectroscopy or  $3.6 \mu\text{m}$  matches as a function of  $R_C$ -band magnitude. At  $3.6 \mu\text{m}$ , the  $2 \sigma$  depth is  $\sim 1 \mu\text{Jy}$  (for a passive galaxy at  $z = 0.4$ , this corresponds to a stellar mass of  $\sim 9 \times 10^8 M_{\odot}$ ).

The goal is to construct a  $0.3 \leq z \leq 0.48$  mass-selected sample for which representative spectroscopy is available and to reach a required depth at  $8 \mu\text{m}$  to distinguish passive galaxies from those with excess emission at  $8 \mu\text{m}$  ( $2 \sigma$  depth of  $\sim 10 \mu\text{Jy}$ ). Effectively, these criteria set the mass limit to  $2 \times 10^{10} M_{\odot}$ , well above the  $3.6 \mu\text{m}$  limit (§ 2.4 for more details).

## 2.3. Deriving Stellar Masses and MIR Colors

### 2.3.1. Stellar Mass

Near-infrared (NIR) light is a useful tracer of stellar mass because of the weak dependence on star formation history (Aaronson et al. 1979; Rix & Rieke 1993; Bell & de Jong 2001). The  $3.6 \mu\text{m}$  flux has been converted into luminosity and thence to stellar mass following Balogh et al. (2007). To give a brief overview of this procedure: Observed-frame AB luminosities are computed for the assumed cosmology, and an empirical  $k$ -correction is applied to correct to a consistent rest frame of a  $z = 0.4$  galaxy. In this paper we will call this  $^{0.4}[3.6]$ . Secondary corrections are then applied to move into the  $K$ -band rest frame. These corrections are calibrated for objects with both  $[3.6]$  and  $K$ -band photometry (not used in this paper). The mass-to-light ratio of each galaxy in the  $K$  band ( $M_*/L_K$ ) is estimated using a combination of two simple Bruzual & Charlot (2003) models with a Chabrier (2003) IMF. For blue galaxies ( $B - V < 0.4$ ) a constant star formation model with dust extinction  $\tau_v = 1$  mag gives  $M_*/L_K = 0.2$ . For red galaxies ( $B - V > 1.0$ ), a 11.7 Gyr old, dust-free single stellar population model gives  $M_*/L_K = 0.7$ . For intermediate colors a linear interpolation between these values is used. For more details please refer to Balogh et al. (2007). This means that the full range of galaxy types only exhibit a range in  $M_*/L_K$  (and thus also  $M_*/L_{0.4[3.6]}$ ) of 3.5. Therefore, our results are relatively insensitive to whether we select in mass or  $^{0.4}[3.6]$  luminosity. We prefer to select in mass, as it is the more physical quantity and, thus, allows a comparison with the literature.

### 2.3.2. MIR Color

The two template spectra in the top panel of Figure 1 demonstrate the diversity and wealth of spectral information at MIR

<sup>8</sup> See [swire.ipac.caltech.edu/swire/astronomers/publications](http://swire.ipac.caltech.edu/swire/astronomers/publications).

<sup>7</sup> Measured by combining larger aperture measurements for isolated stars with IRAC Data Handbook values. Corrections are 1.184, 1.180, 1.249, and 1.404 for IRAC bands 1–4, respectively.

<sup>9</sup> IRAF is distributed by the National Optical Astronomy Observatories, which are operated by the Association of Universities for Research in Astronomy, Inc., under cooperative agreement with the National Science Foundation.

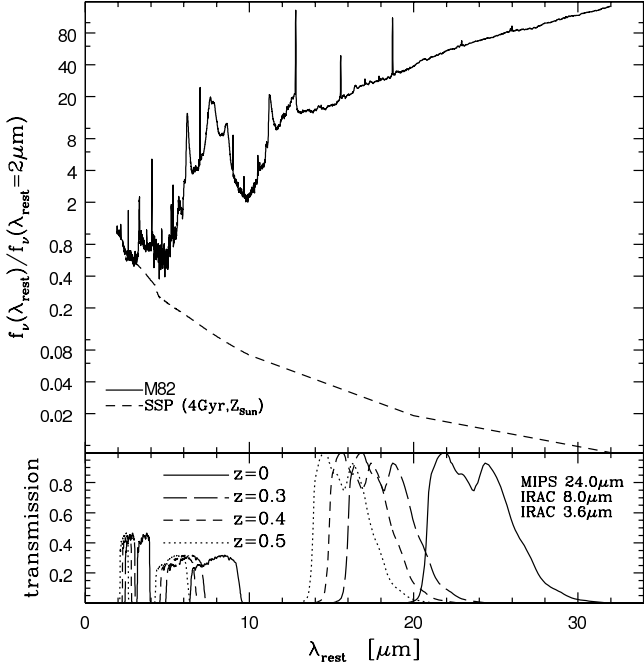


FIG. 1.—Our two MIR spectral templates are illustrated in the top panel. A 4 Gyr old simple stellar population traces pure stellar atmospheric emission from old stars (SSP; *dashed line*). This is generated using PEGASE2 (Fioc & Rocca-Volmerange 1997), with solar metallicity and a Salpeter (1955) IMF with upper mass limit of  $120 M_{\odot}$ . The other template is the ISO-SWS spectrum of the dusty star-forming galaxy M82 (*solid line*; Förster Schreiber et al. 2001). The data are limited to  $\lambda \geq 2.4 \mu\text{m}$ , and so we extrapolate down to  $1.9 \mu\text{m}$  by combining them with the spectrum obtained from a composite stellar population model (constant star formation rate, evolving metallicity, 1 Gyr since start of star formation, Salpeter IMF with upper mass limit of  $120 M_{\odot}$ ). The two templates are normalized to match at  $\lambda = 2.2 \mu\text{m}$ . Beyond  $\sim 3 \mu\text{m}$ , the spectrum of M82 is dominated by dust emission in the form of PAH features ( $\leq 12 \mu\text{m}$ ) and a warm dust emission continuum ( $\geq 12 \mu\text{m}$ ). The bottom panel shows the transmission functions of *Spitzer* IRAC bands at  $3.6$  and  $8 \mu\text{m}$  and the MIPS  $24 \mu\text{m}$  band in the rest frames of galaxies at  $z = 0$  (*solid line*), and  $z = 0.3$  (*long dashed line*),  $0.4$  (*short dashed line*), and  $0.5$  (*dotted line*), corresponding to the redshift range of our galaxies. While  $3.6 \mu\text{m}$  traces stellar emission,  $8$  and  $24 \mu\text{m}$  trace PAH and warm dust emission, respectively, at  $z \sim 0.4$ .

wavelengths. A passive, dust-free galaxy is likely to exhibit a spectrum similar to the simple stellar population (SSP) template (*dashed line*). With no dust emission, the infrared emission originates solely from photospheres of the cold stellar population, primarily giant M stars. Conversely, the spectrum of a dusty star-forming galaxy should look more like that of M82 (*solid line*). Beyond  $\lambda_{\text{rest}} \sim 3\text{--}4 \mu\text{m}$ , a typical dust emission spectrum with characteristic PAH features comes to dominate the M82 template.

The lower panel of Figure 1 shows the transmission function of the IRAC bands at  $3.6$  and  $8 \mu\text{m}$  and the MIPS (Multiband Imaging Photometer for *Spitzer*; Rieke et al. 2004)  $24 \mu\text{m}$  band. Each transmission function is transformed to indicate the rest-frame wavelength domain probed for a galaxy located at  $z = 0.3$ ,  $0.4$ , or  $0.5$ . It is clear that excess (enhanced beyond pure stellar photospheric) emission can be revealed at both  $8$  and  $24 \mu\text{m}$  for galaxies within the redshift range of interest. For  $0.05 \lesssim z \lesssim 0.48$  galaxies the  $8 \mu\text{m}$  band captures the strong  $6.2 \mu\text{m}$  PAH feature, tracing star formation (e.g., Peeters et al. 2004; Förster Schreiber et al. 2004). Crucially, stellar atmospheric emission drops off significantly from  $8$  to  $24 \mu\text{m}$ : thus, detection of passive galaxies, and thence accurate separation of passive from star-forming or AGNs host galaxies, requires much shallower exposure at  $8 \mu\text{m}$  than at  $24 \mu\text{m}$ . A color constructed from  $8$  and  $3.6 \mu\text{m}$  has the

leverage on the galaxy spectrum to make this distinction. In this paper we focus on IRAC data for these reasons.

For the sake of simplicity we compute  $k$ -corrected MIR colors of our galaxies using a linear combination of the two simple templates in Figure 1 (similar to the approach of Huang et al. 2007). We define our color to be the flux ratio  $[f(8)/f(3.6)]$ .<sup>10</sup> For each galaxy, the quantity  $\eta$  is measured: this is the required fractional contribution from the M82 template to match the *observed frame*  $^z[f(8)/f(3.6)]$ .<sup>11</sup> Our  $k$ -corrections are based on the assumption that  $\eta$  (approximately *dust-to-stellar flux ratio*) would be the same regardless of the redshift of the galaxy (and thus the part of the spectrum sampled). The variable  $\eta$  is computed as

$$\eta = \frac{^z[f(8)/f(3.6)] - ^z[f(8)/f(3.6)](\text{SSP})}{^z[f(8)/f(3.6)](\text{M82}) - ^z[f(8)/f(3.6)](\text{SSP})}. \quad (1)$$

To minimize the  $k$ -corrections  $^z[f(8)/f(3.6)]$  is transformed to the equivalent color for a  $z = 0.4$  galaxy, and we limit ourselves to galaxies in the narrow redshift range  $0.3 \leq z \leq 0.48$ , an epoch  $\gtrsim 3$  Gyr ago. The  $k$ -corrected  $[f(8)/f(3.6)]$  color is computed as

$$^{0.4}[f(8)/f(3.6)] = \eta \times ^{0.4}[f(8)/f(3.6)](\text{M82}) + (1 - \eta) \times ^{0.4}[f(8)/f(3.6)](\text{SSP}). \quad (2)$$

A pure SSP  $k$ -correction ( $< 0.07^z[f(8)/f(3.6)]$ ) increases by  $\lesssim 10\%$  going from ages of  $8\text{--}1$  Gyr and  $10\%\text{--}20\%$  going from solar to 3 times solar metallicity. For  $\eta = 1$  (M82-like)  $^{0.4}[f(8)/f(3.6)] = 2.17$  ( $\sim 7$  times the stellar photospheric continuum emission within the IRAC  $8 \mu\text{m}$  band). While  $k$ -corrections of high- $\eta$  galaxies are more uncertain due to the assumed M82 template,  $k$ -corrections remain relatively small within our redshift range ( $\lesssim 50\%$  for  $\eta = 1$ ). In this paper we will only separate dusty galaxies emitting excess light at infrared wavelengths from passive galaxies and will not draw strong conclusions from precise MIR colors of dusty galaxies that are sensitive to the applied  $k$ -correction. To this extent, we believe that we are justified in applying these rough  $k$ -corrections.

#### 2.4. A Mass-Selected Sample

In this paper our analysis is limited to the subsample of galaxies with known redshifts  $0.3 \leq z \leq 0.48$  and with full IRAC coverage. Of these, the 333 galaxies with stellar masses  $M_* > 2 \times 10^{10} M_{\odot}$  are selected, corresponding to a luminosity of  $^{0.4}[3.6] = -20.89$  for passively evolving galaxies, or a flux of  $f(3.6 \mu\text{m}) > 20 \mu\text{Jy}$ , well above the detection limit.

This stellar mass limit is actually defined by the depth of the  $8 \mu\text{m}$  data, since we require this color information for our analysis. In our mass-limited sample, 313 of the 333 galaxies are detected ( $2 \sigma$ ) at  $8 \mu\text{m}$ , and the remainder have  $> 1.8 \sigma$  upper limits that are sufficient to identify them as passively evolving galaxies, characterized by colors  $^{0.4}[f(8)/f(3.6)] < 0.5$  (see § 3 for a justification of this definition).

The requirement that all galaxies have a spectroscopic redshift introduces sensitivity to the optical ( $R_C$ ) selection function. To account for selection bias, the spectroscopic selection weight  $W$

<sup>10</sup> For a more traditional color, simply compute  $[3.6] - [8] = +2.5 \log_{10}[f(8)/f(3.6)]$ .

<sup>11</sup> The prefix superscript  $z$  is used to indicate the bandpass (Blanton & Roweis 2007), i.e., the redshift of a galaxy for which the  $k$ -correction is defined to be 0.

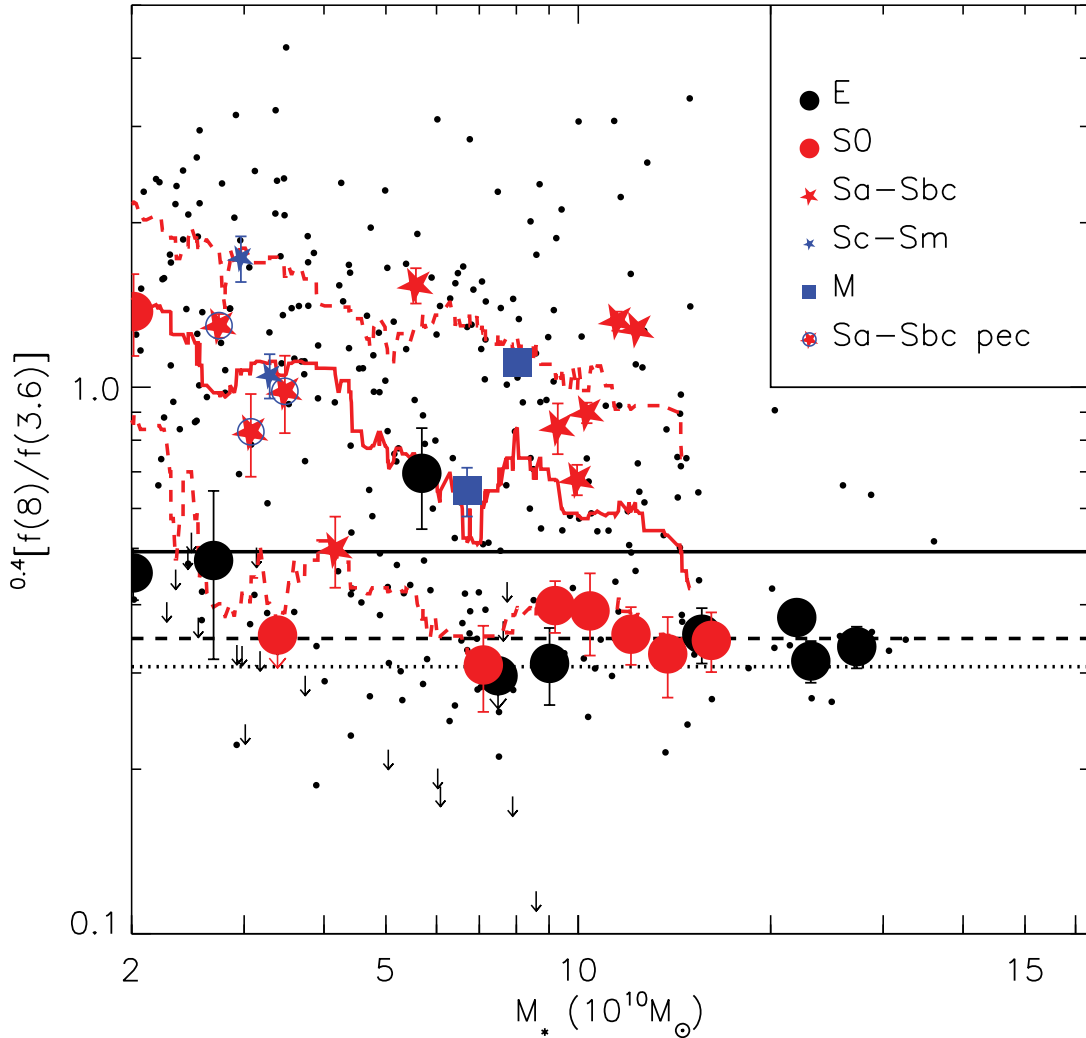


FIG. 2.—The  $^{0.4}[f(8)/f(3.6)]$ - $M_*$  “color-mass” plane for our sample of  $333 M_* \geq 2 \times 10^{10} M_\odot$ ,  $0.3 \leq z \leq 0.48$  galaxies. For the few galaxies without  $2\sigma$   $8\ \mu\text{m}$  detections,  $2\sigma$  upper limits on  $^{0.4}[f(8)/f(3.6)]$  are indicated. The 25th, 50th, and 75th percentiles of the  $^{0.4}[f(8)/f(3.6)]$  distribution are overplotted (red solid and red dashed lines). These are unweighted, and computed for running bins of 50 galaxies in  $M_*$ , and undetected galaxies are considered to be located at their measured values as opposed to upper limit values. Larger symbols are used for galaxies in the joint IRAC-ACS sample for which galaxies are morphologically classified (see key). For morphologically classified galaxies, measurement errors on  $^{0.4}[f(8)/f(3.6)]$  are shown, which are typical of the overall population. Early-type galaxies cluster along a tight sequence at  $^{0.4}[f(8)/f(3.6)] \sim 0.35$ , consistent with pure stellar photospheric emission (horizontal dashed line). We call this the IPS and define (IRE) galaxies as those with  $^{0.4}[f(8)/f(3.6)] > 0.5$  (horizontal solid line). The SSP template is indicated by the horizontal dotted line ( $^{0.4}[f(8)/f(3.6)] = 0.308$ ).

is applied (§ 2.1). This weight includes the factor  $W_z$ , which applies a volume correction to correct for galaxies that fall out of the  $R_C \leq 21.5$  sample at  $z_{\text{lim}} \leq 0.48$ . Within a  $M_* \geq 2 \times 10^{10} M_\odot$  sample, the lowest mass and highest redshift galaxies with high mass-to-light ratios will not make this magnitude cut. Nonetheless, the weighted sample is still representative: A passively evolving  $M_* = 2 \times 10^{10} M_\odot$  galaxy can be sampled with  $R_C \leq 21.5$  up to a redshift of  $z_{\text{lim}} \sim 0.38$  ( $\sim 36\%$  of the volume sampled) and receives a weight  $W_z = 1.0/0.36 = 2.78$ . There do exist four  $R_C \leq 21.5$  galaxies with unusually high mass-to-optical light ratios. These can more easily be lost from the sample due to their extremely red optical-NIR colors. Such red colors can exist where there is extreme dust extinction or a population of AGB stars boosting NIR luminosity. However, they are too few to significantly influence our statistics. Our sample of 333 galaxies includes 11  $M_* > 2 \times 10^{10} M_\odot$  galaxies with  $R_C > 21.5$ . These are assigned zero weight, but it is worth noting that the IRE fraction of these optically faint galaxies is comparable to that of other galaxies. In practice, our results are not strongly sensitive to the statistical weights.

### 3. BIMODAL MIR COLORS AND A PASSIVE SEQUENCE

In this section the distribution of the MIR color  $^{0.4}[f(8)/f(3.6)]$  and its dependence on galaxy stellar mass  $M_*$  are investigated. Figure 2 shows how the 333 galaxies in our  $M_* \geq 2 \times 10^{10} M_\odot$ ,  $0.3 \leq z \leq 0.48$  sample populate the  $^{0.4}[f(8)/f(3.6)]$ - $M_*$  “color-mass” plane, along with the 25th, 50th, and 75th percentiles of the distribution.

The distribution shifts to lower  $^{0.4}[f(8)/f(3.6)]$  with higher mass. Dust flux per unit stellar mass can be approximated by  $^{0.4}[f(8)/f(3.6)] - 0.308$ , where the stellar atmospheric contribution to  $^{0.4}[f(8)/f(3.6)]$  is estimated by the SSP template to be  $^{0.4}[f(8)/f(3.6)](\text{SSP}) = 0.308$  (dotted line). The median relation between  $^{0.4}[f(8)/f(3.6)] - 0.308$  and stellar mass can be well fit by a linear relation in log space:  $\log_{10}\{^{0.4}[f(8)/f(3.6)]_{50\%} - 0.308\} = (8.8 \pm 0.2) - (0.85 \pm 0.02) \log_{10}(M_*/M_\odot)$ . This relation is significantly shallower than would be expected for no relation between dust flux and stellar mass ( $^{0.4}[f(8)/f(3.6)] - ^{0.4}[f(8)/f(3.6)](\text{SSP}) \sim 1/M_*$ ). However, this is sensitive to the exact value of  $^{0.4}[f(8)/f(3.6)](\text{SSP})$  chosen.

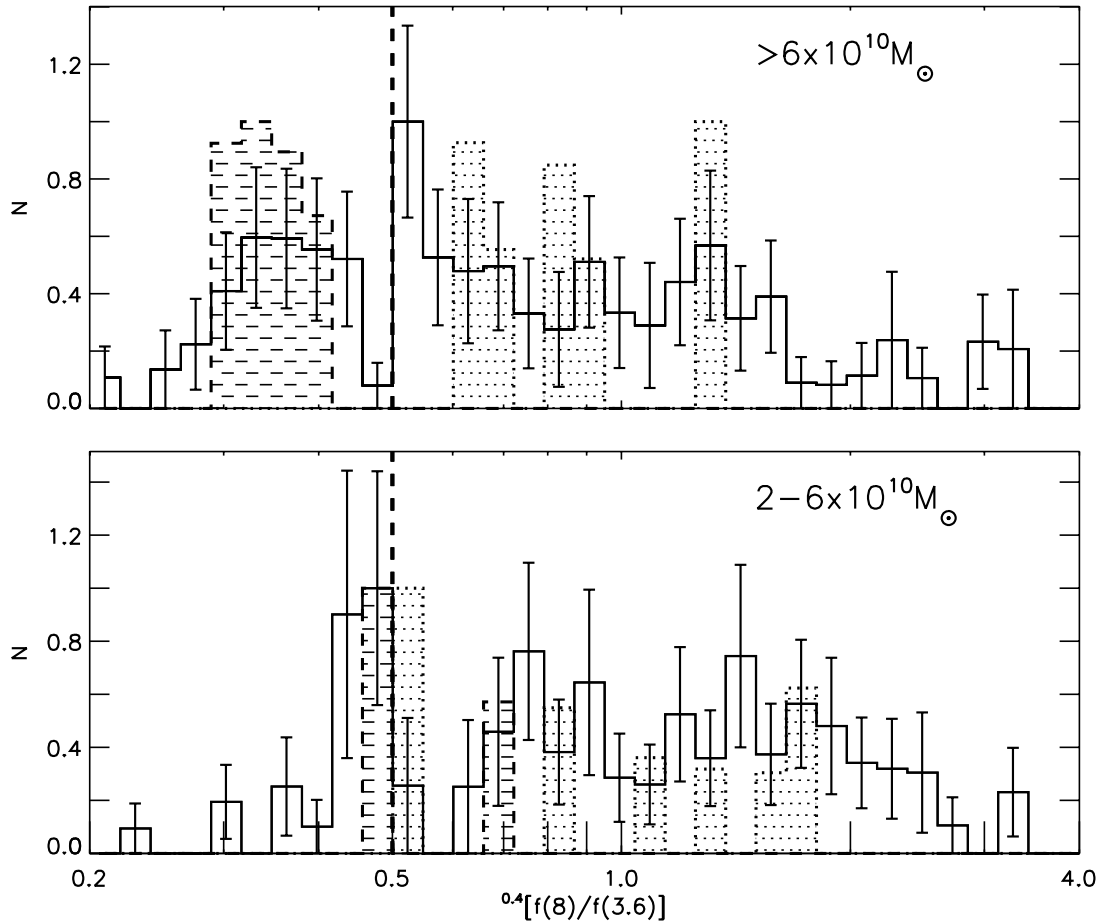


FIG. 3.— Weighted distribution of the MIR color  $^{0.4}[f(8)/f(3.6)]$  for  $0.3 \leq z \leq 0.48$  galaxies with  $M_* > 6 \times 10^{10} M_\odot$  (top) and  $M_* = (2-6) \times 10^{10} M_\odot$  (bottom), binned in log space and with Poissonian error bars. The few galaxies without  $2\sigma$  detections at  $8\ \mu\text{m}$  are excluded. Since these are all constrained at the  $\geq 1.8\sigma$  level to lie at  $^{0.4}[f(8)/f(3.6)] < 0.5$ , their inclusion would not destroy the bimodality. Overplotted are the distributions for morphologically classified early-type (dash-filled histogram) and late-type (dot-filled histogram) galaxies, renormalized to give the same maximum value. Our criterion for an IRE galaxy ( $^{0.4}[f(8)/f(3.6)] = 0.5$ ) is indicated with the vertical dashed line and effectively separates the peak of the IPS ( $^{0.4}[f(8)/f(3.6)] < 0.5$ ) from the IRE galaxy population.

We also examine whether the strong correlation between MIR activity and morphology observed in the local universe (Pahre et al. 2004a; Li et al. 2007) extends to our intermediate redshift sample. Thirty-one of the galaxies in our sample are within the ACS fields and have been morphologically classified by AO. These are indicated in Figure 2.

Morphologically classified early-type (elliptical and S0) and late-type (mainly spiral) galaxies exhibit very different MIR color distributions, as seen locally by Li et al. (2007). In fact, the overall distribution in  $^{0.4}[f(8)/f(3.6)]$  is bimodal in nature, with the two peaks in MIR color almost equivalent to these two morphological classes. This bimodality has been observed in other (local) optical-NIR-selected samples (Li et al. 2007; Johnson et al. 2007), while it is less obvious in shallow  $8\ \mu\text{m}$ -selected samples, where early types are more difficult to detect (Huang et al. 2007). The bimodality of CNOC2 galaxies is demonstrated in Figure 3, split into two bins of stellar mass. Within each mass range there exists a significant population of galaxies with  $^{0.4}[f(8)/f(3.6)] < 0.5$  and then a gap before the onset of a second population of galaxies emitting more strongly at  $8\ \mu\text{m}$ . While the full distribution seems to shift to higher  $^{0.4}[f(8)/f(3.6)]$  at lower mass, the value  $^{0.4}[f(8)/f(3.6)] = 0.5$  is within the gap across our mass range. Thus, we adopt this value to divide the sample: everything with  $^{0.4}[f(8)/f(3.6)] > 0.5$  we call an IRE galaxy. This division at 0.5 excludes galaxies from the passive population if they have 44% more  $8\ \mu\text{m}$  flux than the early-type locus. Contributions

from circumstellar dust (Piovan et al. 2003; Temi et al. 2008) or silicate emission from mass loss (Bressan et al. 2007) are unlikely to produce such a strong boost to the  $8\ \mu\text{m}$  flux.

The dash-filled histogram in Figure 3 indicates the  $^{0.4}[f(8)/f(3.6)]$  distribution for morphologically early-type galaxies. The tight distribution of high-mass early types is mirrored in the narrow locus of almost constant color in the color-mass plane (Fig. 2). The 11 early types (ignoring the single upper limit) with  $M_* > 6 \times 10^{10} M_\odot$  have mean color and scatter  $^{0.4}[f(8)/f(3.6)] \sim 0.347 \pm 0.03$  (Fig. 2, horizontal dashed line). The scatter is consistent with the photometric errors. We call this the IPS, which is not far offset from the template SSP color ( $^{0.4}[f(8)/f(3.6)] = 0.308$ , horizontal dotted line). The peak value and scatter of the IPS for the full population of  $M_* > 6 \times 10^{10} M_\odot$  galaxies is  $^{0.4}[f(8)/f(3.6)] \sim 0.34 \pm 0.05$ . The tight scatter of the IPS is reminiscent of the optical red sequence (e.g., Bower et al. 1992). Indeed, the tightness of the IPS is due to the emission from stellar atmospheres of cold stars in passive galaxies, which has relatively little sensitivity to age or metallicity. Mid-infrared wavelengths are highly sensitive to dust emission; thus, the infrared passive sequence does not suffer from the degeneracy between dusty red galaxies and passive red galaxies as does a red sequence defined at optical wavelengths.

The second, broader peak at  $^{0.4}[f(8)/f(3.6)] > 0.5$  contains IRE galaxies with excess (nonstellar) emission at  $8\ \mu\text{m}$ . This excess emission traces some kind of activity, i.e., star formation or AGN.

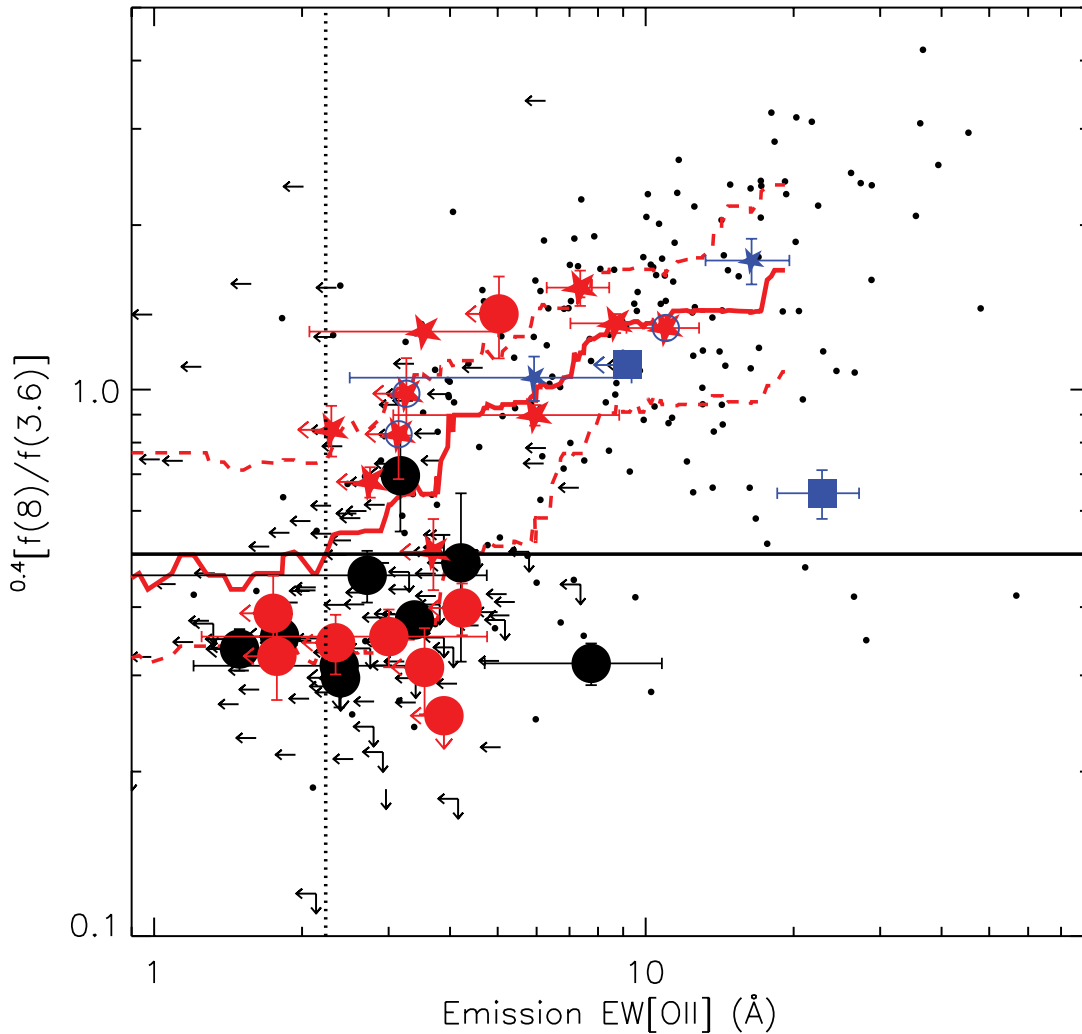


FIG. 4.—The  $^{0.4}[f(8)/f(3.6)]$ -EW[O II] plane for 319  $M_* \geq 2 \times 10^{10} M_\odot$  and  $0.3 \leq z \leq 0.48$  galaxies. The 25th, 50th, and 75th percentiles of the  $^{0.4}[f(8)/f(3.6)]$  distribution are overplotted, computed over running bins of 50 galaxies in EW[O II] (red solid, and red dashed lines). Undetected galaxies (at the  $1 \sigma$  level in [O II] or the  $2 \sigma$  level at  $8 \mu\text{m}$ ) are plotted at their EW[O II] ( $1 \sigma$ ) and  $^{0.4}[f(8)/f(3.6)]$  ( $2 \sigma$ ) upper limit levels (arrows), while the percentiles are computed based on *measured* [O II] and  $8 \mu\text{m}$  flux levels: on a statistical basis the 50th percentile should therefore be representative of the true median relation (both measured [O II] and  $8 \mu\text{m}$  flux can be negative for nondetections). Our empirical division ( $^{0.4}[f(8)/f(3.6)] = 0.5$ ) is overplotted (solid horizontal line). There is a strong correlation between EW[O II] and  $^{0.4}[f(8)/f(3.6)]$ , inferring that for the average galaxy both diagnostics trace the same phenomenon (primarily star formation). The median galaxy at our empirical division  $^{0.4}[f(8)/f(3.6)] = 0.5$  has EW[O II] =  $2.1 \text{ \AA}$  (dotted vertical line). Larger symbols are used for morphologically classified galaxies as in Fig. 2, with measurement errors typical of the overall population.

Figures 2 and 3 show that all known late-type galaxies (Fig. 3, *dot-filled histogram*) in the sample inhabit this peak. Two morphologically classified early-type galaxies also exhibit excess emission at  $8 \mu\text{m}$ . Excess MIR emission in some early-type galaxies is known to exist and correlates with low levels of star formation or AGN activity (e.g., Pahre et al. 2004b; Bressan et al. 2007).

#### 4. THE $^{0.4}[f(8)/f(3.6)]$ -EW[O II] PLANE

It is useful to compare the MIR color  $^{0.4}[f(8)/f(3.6)]$  with an independent, well-studied indicator of activity (primarily star formation), the equivalent width of the [O II]  $\lambda 3727$  emission line. [O II] is most commonly used at  $z \gtrsim 0.3$ , where the H $\alpha$   $\lambda 6563$  emission line is redshifted out of the optical window. By normalizing the emission flux by the continuum level, the sensitivity to flux calibration and dust absorption is reduced, producing a normalized quantity more easily comparable to  $^{0.4}[f(8)/f(3.6)]$ .

Figure 4 shows the location of our  $M_* \geq 2 \times 10^{10} M_\odot$  and  $0.3 \leq z \leq 0.48$  galaxies (excluding 14 galaxies where EW[O II] could

not be measured) in the  $^{0.4}[f(8)/f(3.6)]$ -EW[O II] plane, including the 25th, 50th, and 75th percentiles and morphologically classified galaxies overplotted with their errors.

There is a strong correlation between EW[O II] and  $^{0.4}[f(8)/f(3.6)]$ . Both diagnostics trace galaxy activity, and primarily star formation, and so a strong correlation is expected. A value of EW[O II] =  $2.1 \text{ \AA}$  (dotted vertical line) corresponds to the median galaxy with  $^{0.4}[f(8)/f(3.6)] = 0.5$  (our empirical division in MIR color; solid horizontal line), which is below the [O II] detection limit of most spectroscopic surveys. Indeed, we are only able to identify this value for a large statistical sample: the median error on EW[O II] for individual galaxies in our sample is  $2.4 \text{ \AA}$ .

In Balogh et al. (2007) we divided our sample into passive and [O II] strong galaxies at EW[O II] =  $10 \text{ \AA}$ . This is the equivalent of a division at  $^{0.4}[f(8)/f(3.6)] = 1.31$  for the median galaxy, selecting only the tail of galaxies with the most ongoing activity. A division at EW[O II] =  $5 \text{ \AA}$  (as used in Wilman et al. 2005) corresponds to  $^{0.4}[f(8)/f(3.6)] = 0.92$ . Therefore, with a reasonable photometric depth at  $\lambda_{\text{rest}} \sim 6 \mu\text{m}$ , it is possible to pick up

levels of activity not possible without extremely deep optical spectroscopy. This inevitably leads to a higher fraction of galaxies defined as nonpassive. Many spiral galaxies (mainly of type Sa–Sbc) with  $^{0.4}[f(8)/f(3.6)] > 0.5$  have no detectable [O II] emission. Based on a simple cut in EW[O II], these would be classified as passive spirals (e.g., Poggianti et al. 1999; Balogh et al. 2002). It is now clear that most such galaxies are not truly passive (in the sense of the IPS galaxies); instead, there is evidence at  $8\ \mu\text{m}$  of some ongoing activity. This indicates that the morphological transformation is more intimately linked to (and concurrent with) the complete cessation of star formation than previously believed.

The distribution of galaxies in the  $^{0.4}[f(8)/f(3.6)]$ –EW[O II] plane exhibits a lot of scatter around the median relation. Both EW[O II] and  $^{0.4}[f(8)/f(3.6)]$  are highly sensitive to the presence of dust (through extinction of the [O II] emission by dust, and abundance of PAH carriers), which is itself dependent on the galaxy mass and star formation rate (Giovannelli et al. 1995; Wang & Heckman 1996; Masters et al. 2003; Brinchmann et al. 2004). Thus, while MIR diagnostics are better at tracing activity in high-mass galaxies, activity in lower mass galaxies may be better traced with optical diagnostics (especially at significantly subsolar metallicity and thus very low mass where PAH features disappear; Engelbracht et al. 2005; Draine et al. 2007). However, within the mass range traced here, the median relation for EW[O II] goes as  $\sim M_*^{-0.8}$ , similar to the dependence of  $^{0.4}[f(8)/f(3.6)]$  (once corrected for the stellar atmospheric contribution). To compute EW[O II], the [O II] line flux is normalized by the continuum at  $3727\ \text{\AA}$ , which will lead to a shallower slope than would a normalization by mass. It is likely that this effect counters any steeper relation expected due to different dust dependencies. Therefore, other physical parameters are necessary to drive the scatter in the  $^{0.4}[f(8)/f(3.6)]$ –EW[O II] plane, together with large measurement errors.

There exists a strange population of galaxies extending to high EW[O II] at low  $^{0.4}[f(8)/f(3.6)]$ . These galaxies diverge from the usual situation in massive galaxies: namely, that infrared data trace activity to much lower levels than emission lines. For two of the four galaxies with  $^{0.4}[f(8)/f(3.6)] \leq 0.5$  and EW[O II]  $> 20\ \text{\AA}$ , the redshift depends on a single emission line and might therefore be incorrect. Another possibility is that the [O II] emission originates in a low-mass/metallicity galaxy that is falsely matched to a bright IRAC source. Visual checks suggest that this is unlikely but cannot be certain. Alternatively, these galaxies might be unusually bright at  $3.6\ \mu\text{m}$  for their mass or metallicity. This may occur in metal-poor high-mass galaxies (weird) or galaxies with a strong and very hot AGN component contributing most significantly to the  $3.6\ \mu\text{m}$  band (and AGN activity can also boost the [O II] emission; Yan et al. 2006). The only morphologically classified galaxy at high EW[O II] and low  $^{0.4}[f(8)/f(3.6)]$  is a merger galaxy. This could be explained by either of the above scenarios or a third scenario in which a merger-driven starburst produces such a hard radiation field that it is capable of destroying the PAH carriers. Whatever their origin, these galaxies form a puzzling, possibly interesting, but small minority.

## 5. FREQUENCY OF INFRARED EXCESS MASSIVE GALAXIES

Within our representative sample of  $0.3 \leq z \leq 0.48$  and  $M_* \geq 2 \times 10^{10} M_\odot$  galaxies, we now measure the fraction of infrared excess galaxies,  $f(\text{IRE})$ . Activity is traced with  $^{0.4}[f(8)/f(3.6)]$  down to very low levels at which both star formation and nuclear activity play a role. We will not distinguish between these two forms of activity in this paper, instead merely computing the total fraction of IRE galaxies. However, any galaxy that has gas ac-

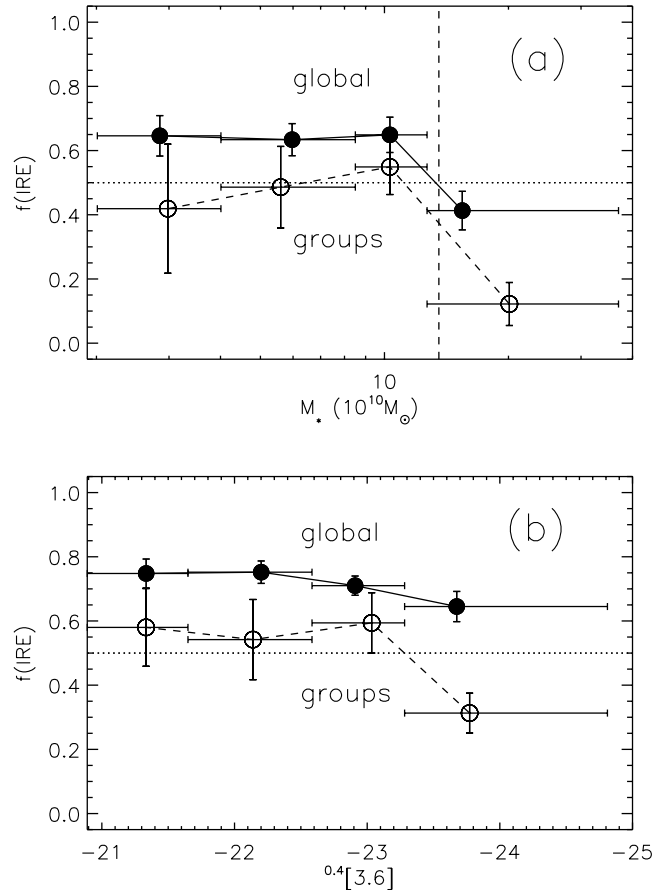


FIG. 5.—(a) Dependence of  $f(\text{IRE})$  (the fraction of IRE galaxies defined by  $^{0.4}[f(8)/f(3.6)] > 0.5$ ) for galaxies at  $0.3 \leq z \leq 0.48$ , divided into four bins of stellar mass ( $M_*$ ). This is computed for the full (global) sample (solid line, filled circles) and the group galaxy sample (dashed line, open circles). Points are plotted at the median  $M_*$  of galaxies in each bin, and errors on  $f(\text{IRE})$  are computed using a bootstrapping method (see text). There is a significant deficit of IRE galaxies in groups, which nonetheless mirror the stellar mass dependence of the global population [ $f(\text{IRE})$  decreases at high mass]. A “crossover mass” ( $M_{\text{cr}}$ ) at which  $f(\text{IRE}) = 0.5$  (dotted horizontal line) is defined: for the global sample  $M_{\text{cr}} \sim 1.3 \times 10^{11} M_\odot$  (dashed vertical line). (b) As (a), except  $f(\text{IRE})$  is plotted against  $^{0.4}[3.6]$  luminosity for galaxies in a luminosity-limited sample.

creting onto a supermassive black hole is likely to be simultaneously forming stars (Brinchmann et al. 2004; Berta et al. 2007; Shi et al. 2007). Hence, such galaxies are correctly distinguished from the passive population.

To measure  $f(\text{IRE})$ , the fraction of galaxies with  $^{0.4}[f(8)/f(3.6)] > 0.5$  is computed, with galaxies weighted to account for the magnitude-dependent selection function (§ 2.4). The application of this weight does not significantly change the results. To place errors on  $f(\text{IRE})$  we perform bootstrap resampling of the sample. This is done by creating 1000 independent samples of the same size as the true sample: within each sample, values of  $^{0.4}[f(8)/f(3.6)]$  are taken randomly and often repeatedly from the true sample and scattered using a Gaussian kernel of width equal to the error on  $^{0.4}[f(8)/f(3.6)]$ . The standard deviation of  $f(\text{IRE})$  from the bootstrap samples is taken for the error on  $f(\text{IRE})$ .

Figure 5a (filled circles and solid line) shows  $f(\text{IRE})$  binned by stellar mass for the global population. Bins are not equally populated. Instead, they are defined such that there is an approximately equal number of group galaxies per bin (§ 6). The  $^{0.4}[f(8)/f(3.6)]$  declines with  $M_*$ , an effect seen previously in the median and percentiles. However, this is only evident in the highest mass bin.

To test for effects of cosmic variance, this exercise is repeated independently for each of the three CNOC2 patches with IRAC coverage.<sup>12</sup> The patch-to-patch offsets in  $f(\text{IRE})$  are  $\lesssim 3\%$ , compatible with the bootstrap errors and indicating that cosmic variance is not a dominant source of error. Therefore, this result is robust.

The *crossover mass* [ $M_{\text{cr}}$ , where  $f(\text{IRE}) = 0.5$ ; Fig. 5a, dotted horizontal line], is  $M_{\text{cr}} \sim 1.3 \times 10^{11} M_{\odot}$  (Fig. 5a, dashed vertical line). Hopkins et al. (2007) compiled estimates of  $M_{\text{cr}}$  (their “ $M_{\text{tr}}$ ”) at different redshift. These are scaled to a Chabrier IMF and our cosmological parameters for comparison with our measurement. Defining  $M_{\text{cr}}$  as the stellar mass at which 50% of galaxies are optically blue or have a high specific star formation rate (calibrated using emission lines), they measure  $M_{\text{cr}} \sim (1.6\text{--}3.8) \times 10^{10} M_{\odot}$  at  $z \sim 0.4$ , almost an order of magnitude lower than our estimate. This probably reflects our sensitivity to low levels of star formation in high-mass galaxies. However, a definition of 50% morphologically late-type galaxies results in an estimate of  $M_{\text{cr}} \sim (3\text{--}8) \times 10^{10} M_{\odot}$  at  $z \sim 0.4$ , much more compatible with our value within errors. This suggests that morphological selection is identifying more or less the same population as infrared selection. This is interesting, as it tells us that morphological transformation usually goes hand in hand with the final truncation of star formation in massive galaxies.

## 6. THE GROUP ENVIRONMENT

We will now examine how the fraction of infrared excess galaxies depends on the group environment by computing  $f(\text{IRE})$  for group galaxies as a function of stellar mass. Groups were detected as overdensities in redshift space by applying a friends-of-friends algorithm to the CNOC2 redshift survey (Carlberg et al. 2001). Membership has been reassigned after inclusion of additional spectroscopy and application of the membership algorithm defined in Wilman et al. (2005).<sup>13</sup> To ensure that most group galaxies are not interlopers (i.e., nearby galaxies not bound to the group at the time of observation) the sample is limited to those within 500 kpc of the luminosity-weighted group center. The value 500 kpc corresponds to the virial radius for a  $\sim 360 \text{ km s}^{-1}$  group at  $z = 0.4$ . Our decision to select group galaxies within a fixed radial aperture instead of a scaled aperture (e.g., the virial radius) is made because measurements of velocity dispersions are uncertain and known to be heavily biased for systems with  $\lesssim 30$  members (e.g., Zabludoff & Mulchaey 1998). Seventy-eight of 333 galaxies from the mass-selected sample match these group criteria. Of these, 59% are in groups with measured velocity dispersions  $\sigma_{\text{intr}} < 360 \text{ km s}^{-1}$ , 80% are in groups with  $\sigma_{\text{intr}} < 500 \text{ km s}^{-1}$ , and 6% are in the cluster g226 ( $\sigma_{\text{intr}} \sim 850 \text{ km s}^{-1}$ ).

The dashed line and open symbols in Figure 5a show how  $f(\text{IRE})$  depends on stellar mass for group galaxies only. Each bin contains 19 or 20 group galaxies by design and appears to show a deficit of IRE galaxies with respect to the global population. This is not highly significant in individual mass bins but is consistent at all masses. Thus we estimate the combined significance for the whole sample. In groups, the combined value of  $f(\text{IRE})$  is 0.447. As the mass distribution of group galaxies is biased to high mass relative to the global sample, the global sample is resampled to match the group sample on mass. For each group galaxy, a random galaxy is selected from the nearest 10 galaxies in stellar mass (from the global sample, other than itself, and with no repeats).

This resampling process is repeated 10,000 times, each time computing  $f(\text{IRE})$  for the matched sample. On only 56 of 10,000 occasions is  $f(\text{IRE}) \leq 0.447$ . This corresponds to a 0.56% likelihood ( $\sim 2.5 \sigma$  from a one-tailed Gaussian) that the low value of  $f(\text{IRE})$  in groups arises by chance.

The lower value of  $f(\text{IRE})$  in groups *independent of the stellar mass* indicates that activity in  $M_{*} \geq 2 \times 10^{10} M_{\odot}$  galaxies is often suppressed by the group environment. As these groups are predominantly low velocity dispersion, often unvirialized systems, this means that massive galaxies are already affected by the low-mass halo environment. The mechanism of suppression seems to be particularly active in the highest stellar mass bin ( $M_{*} \geq 1.27 \times 10^{11} M_{\odot}$ ), where in groups  $f(\text{IRE}) = 0.12 \pm 0.07$ . In this mass bin the group galaxies also dominate the passive global population: Of a total of 43 galaxies (25 passive), 20 are in our group sample (17 passive). Hence, the most massive galaxies seem to become passive in the group environment. This result is even more remarkable when it is considered that the group sample is incomplete due to incompleteness effects in the CNOC2 redshift survey, so the global sample should include more group galaxies than have been identified.

It is prudent to repeat this exercise as a function of  $^{0.4}[3.6]$  luminosity to ensure that this result does not somehow depend on our mass calibration. Figure 5b shows how  $f(\text{IRE})$  depends on  $^{0.4}[3.6]$  luminosity for a luminosity-selected sample ( $^{0.4}[3.6] \leq -20.89$ ). Luminosity selection allows an additional  $180 M_{*} < 2 \times 10^{10} M_{\odot}$  galaxies to make it into the sample with lower than maximum mass-to-light ratios. Effectively this means that the overall value of  $f(\text{IRE})$  is higher for the luminosity-selected sample ( $0.735 \pm 0.018$ ) than for the mass-selected sample ( $0.621 \pm 0.030$ ). The trends mirror those seen as a function of mass with the exception that in the bin of highest luminosity the global  $f(\text{IRE})$  is still quite high ( $0.645 \pm 0.047$ ). This is because IRE galaxies are more likely to be found in the high-luminosity bin than in the high-mass bin, due to their lower mass-to-light ratios. In groups the dominance of passive galaxies is so strong as to mitigate this effect.

## 7. DISCUSSION

MIR color is a highly sensitive tracer of activity in galaxies. This has allowed us to separate truly passive galaxies (typically morphologically early type) from galaxies with infrared excess at  $8 \mu\text{m}$  (IRE galaxies). In this way we avoid confusion between galaxies with low but still ongoing star formation and those which have shut down their star formation altogether (probably coincident with the morphological transformation). Other studies examine the evolution in fractions of highly star-forming galaxies (LIRGs, ULIRGs, etc.; Bell et al. 2005; Le Floch et al. 2005; Hammer et al. 2005; Caputi et al. 2006; Daddi et al. 2007). These fractions decline steeply with cosmic time, with contributions from generally declining star formation rates in most galaxies and complete suppression in some.

Our main result is that a strong and highly significant deficit in the fraction of infrared excess galaxies,  $f(\text{IRE})$ , exists in optically selected, mostly low velocity dispersion groups at  $z \sim 0.4$  and is *independent of stellar mass*. The suppression of infrared activity in low-redshift Hickson compact groups (Johnson et al. 2007) therefore extends to the “loose group” regime at  $z \sim 0.4$ .

Our group data indicate a dramatic drop in  $f(\text{IRE})$  at stellar masses  $M_{*} \gtrsim 10^{11} M_{\odot}$ . This coincides with the stellar mass at which a galaxy’s own halo usually exceeds  $M_{\text{halo}} \sim 5 \times 10^{12} M_{\odot}$ , which is also the mass of the Local Group (Li & White 2008) and typical of the lower mass groups in our sample (McGee et al.

<sup>12</sup> CNOC2 consists of four patches spaced at intervals of  $\sim 90^{\circ}$  in R.A., of which three are partially mapped by IRAC.

<sup>13</sup> The group aspect ratio,  $b$ , is set to 5.

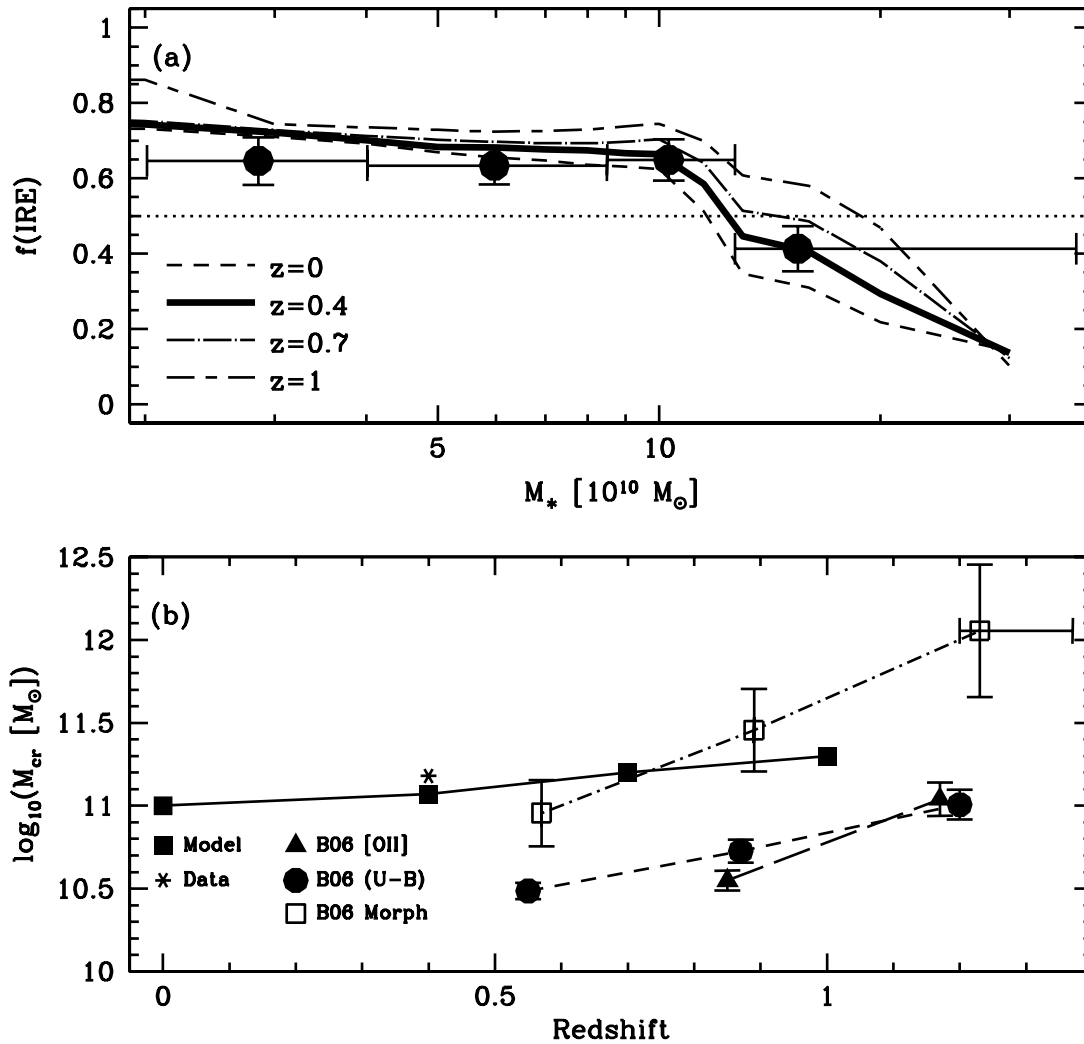


FIG. 6.—(a) Dependence of  $f(\text{IRE})$  on stellar mass  $M_*$  for the global population of  $0.3 \leq z \leq 0.48$  CNOC2 galaxies compared with our simple model predictions at  $z = 0.4$ . The model predictions are also computed at  $z = 0, 0.7$ , and  $1$ . Galaxies in halos with  $M_{\text{halo}} \geq 5 \times 10^{12} M_\odot$  are considered to be in groups. The stellar mass dependence can be reproduced by a model in which suppression of galaxy activity is driven primarily by the group environment. (b) Evolution of the crossover mass  $M_{\text{cr}}$  (where 50% of all galaxies are active, computed in various ways). Our data point [ $M_{\text{cr}}$  at  $z = 0.4$  computed using  $f(\text{IRE}) = 0.5$  in CNOC2] is compared with the model predictions at  $z = 0, 0.4, 0.7$ , and  $1$ , and DEEP2 crossover masses computed in different redshift bins by Bundy et al. (2006, [B06]) for 50% late-type morphologies, 50% galaxies blue in  $(U-B)$  color, and 50%  $[\text{O II}]$ -inferred SFR above  $0.2 M_\odot \text{ yr}^{-1}$ . Our simple model can qualitatively reproduce a downsizing scenario, although the redshift dependence is shallower than observed by B06.

2008). Therefore, galaxies with  $M_* \gtrsim 10^{11} M_\odot$  are typically “central” galaxies in groups, which is why many of our most massive galaxies are members of known groups. *The low-mass group environment suppresses star formation in both central massive galaxies and their satellites. The strongest effect is in the central galaxies.*

In this paper we do not fully constrain the mechanism(s) responsible for suppressing activity in groups. For a discussion of the menagerie of possibilities we refer to Moran et al. (2007, and references therein). The ability to detect low levels of activity has important implications for the interpretation of passive spirals as identified purely from their  $[\text{O II}]$  emission (Poggianti et al. 1999; Balogh et al. 2002; Moran et al. 2006). Our strongest direct constraint on the mechanism(s) at work is that it (they) must be active in low-mass group halos. This probably excludes processes such as ram pressure stripping, which prefer much higher density environments (Gunn & Gott 1972; Quilis et al. 2000).

Relating the suppression of star formation to a halo mass threshold is theoretically attractive, as the physics of gas accre-

tion and feedback are more likely to relate to the gravitationally bound material within the halo than to the stellar mass of the galaxy itself (e.g., Dekel & Birnboim 2006). For example, AGN feedback processes might be especially efficient in galaxies located inside group-sized halos. Brightest group galaxies (BGGs) more frequently contain radio-loud AGNs than similarly massive non-BGGs. This is likely to be related to the cooling of the hot intragroup medium (IGM) onto the BGG, fueling a radio-loud AGNs (Best et al. 2007).

Our data alone are not sufficient to examine how the suppression of star formation within group-mass halos contributes to the global population in a statistical manner. Incompleteness of the CNOC2 redshift survey and uncertainties in the construction of the group catalog and galaxy membership inevitably lead to incompleteness of our group galaxy sample in a way that may depend on galaxy stellar mass. To better estimate membership on a statistical basis, we use a simulated galaxy catalog in which stellar mass and embedding halo mass can be directly evaluated for each galaxy at  $z = 0.4$ . We choose the “mock” galaxy catalog

of Bower et al. (2006), which is based on the millenium simulation, a simulated  $\Lambda$ CDM universe with  $500 h_{100}^{-1}$  Mpc sides (Springel et al. 2005). These dark matter halos are populated with mock galaxies using a semi-analytic technique. Only the positions (environment) and stellar masses of these galaxies are used. The mock galaxies are assumed to be in groups where they are located within halos  $M_{\text{halo}} \geq 5 \times 10^{12} M_{\odot}$ . Mock group galaxies are then assigned a probability that they are IRE galaxies consistent with the data: i.e.,  $f(\text{IRE}) = 0.5$  for the  $M_* < 10^{11} M_{\odot}$  galaxies and  $f(\text{IRE}) = 0.1$  for the  $M_* \geq 10^{11} M_{\odot}$  galaxies (as seen in Fig. 5a). Combined with the rest of the mock galaxy population (“field” galaxies), the dependence of  $f(\text{IRE})$  on stellar mass is compared to the CNOC2 global trend. By setting the fraction of IRE field galaxies to 0.9, regardless of their stellar mass, the global trend is well reproduced. This is demonstrated in Figure 6a in which the observed global trend for CNOC2 galaxies (*filled circles*) is extremely well matched by the model (*solid line*). That the fraction of field galaxies that ‘need to be passive is low (0.1) and independent of stellar mass lends support to our hypothesis that the halo mass is more important than the stellar mass for the suppression of star formation in galaxies.

Figure 6a also shows how  $f(\text{IRE})$  depends on stellar mass for the mock galaxy population evaluated at  $z = 0, 0.7$ , and 1. Remarkably, the model exhibits a *downsizing* behavior, such that the crossover mass  $M_{\text{cr}}$  decreases at lower redshifts. This is shown in Figure 6b with the CNOC2 data point at  $z = 0.4$ . The only reason for this evolution is that the fraction of galaxies in groups increases, as a function of stellar mass, from  $z = 1$  to 0. *Suppression of galaxy activity in groups, plus the gravitational growth of structure in the universe, can explain downsizing trends in  $M_{\text{cr}}$ .*

Also in Figure 6b, the crossover masses computed in different redshift bins by Bundy et al. (2006) are overplotted (reproduced from their Fig. 9;  $M_{\text{cr}}$  is called the “transition mass” in that paper). These measurements are based on the DEEP2 redshift survey and contribute to the compilation of Hopkins et al. (2007). The variable  $M_{\text{cr}}$  is computed for 50% late-type morphologies, 50% galaxies blue in ( $U-B$ ) color, and 50% galaxies with [O II]-inferred SFR above  $0.2 M_{\odot} \text{ yr}^{-1}$ . That more morphologically classified late-type galaxies are detected, resulting in a higher value of  $M_{\text{cr}}$ , is fully in line with our estimate at  $z = 0.4$ , using a sensitive MIR color, well correlated with morphology. While our simple model can qualitatively reproduce a downsizing scenario, comparison with Bundy et al. (2006) suggests that the redshift dependence is probably too shallow. With better constraints at different redshift, a model in which star formation is not immediately suppressed on incorporation of a galaxy into a massive halo might serve to steepen this evolution.

## 8. CONCLUSIONS

From the CNOC2 redshift survey, we have constructed a mass-selected sample of galaxies with known spectroscopic redshifts  $0.3 \leq z \leq 0.48$  and stellar masses  $M_* \geq 2 \times 10^{10} M_{\odot}$ . While the sample is not fully complete, the selection is well understood, and we correct for incompleteness using a simple weighting scheme. Within this sample, the fraction of galaxies with excess emission at  $8 \mu\text{m}$  is computed, which traces star formation or nuclear activity. For galaxies in this sample, the mid-infrared (MIR) color  $^{0.4}[f(8)/f(3.6)]$  has been measured. This is the flux ratio of the  $8 \mu\text{m}$  to  $3.6 \mu\text{m}$  IRAC bands,  $k$ -corrected to a consistent rest frame of a  $z = 0.4$  galaxy. Based on this sample we have shown:

*Infrared passive sequence.*—Old stellar populations (such as found in passively evolving galaxies in which star formation

has been suppressed) exhibit very predictable colors in the  $\sim 2-7 \mu\text{m}$  spectral region (rest frame), tracing the stellar atmospheres of giant M stars. This produces a tight infrared passive sequence (IPS) in the  $^{0.4}[f(8)/f(3.6)]$  color. The IPS does not suffer from the optical red sequence degeneracy between dusty red galaxies and passive red galaxies. The mean IPS color ( $^{0.4}[f(8)/f(3.6)] = 0.34$  at  $M_* > 6 \times 10^{10} M_{\odot}$ ) is consistent with an old stellar population, and the tight scatter (0.03–0.05 at high mass) is consistent with photometric errors. This leaves little room for large variations in metallicity, or additional contributions at  $\sim 6 \mu\text{m}$  from circumstellar or diffuse dust.

*MIR color bimodality.*—The  $^{0.4}[f(8)/f(3.6)]$  distribution is bimodal, consisting of the IPS and a population of galaxies with significant excess emission at  $8 \mu\text{m}$  (infrared excess galaxies). These two populations can be divided at  $^{0.4}[f(8)/f(3.6)] = 0.5$ .

*Morphologies and infrared emission.*—Fifteen of 17 morphologically classified early-type (elliptical or S0) galaxies have  $^{0.4}[f(8)/f(3.6)]$  colors consistent with the IPS, while no classified late-type galaxy has  $^{0.4}[f(8)/f(3.6)] < 0.5$ . This is consistent with known correlations at low redshift between morphology and MIR colors (e.g., Pahre et al. 2004a; Li et al. 2007).

*Tracing low-level activity in the MIR.*—There is a strong correlation between  $^{0.4}[f(8)/f(3.6)]$  and EW[O II]. However, our division at  $^{0.4}[f(8)/f(3.6)] = 0.5$  corresponds to a division at EW[O II] =  $2.1 \text{ \AA}$  for the median galaxy. This is below the [O II] detection limit of most intermediate- to high-redshift surveys. This shows that MIR diagnostics trace low levels of activity at  $z \sim 0.4$ . Consequently, dividing at  $^{0.4}[f(8)/f(3.6)] = 0.5$  selects a high fraction of IRE galaxies,  $f(\text{IRE})$ , and the crossover mass at which  $f(\text{IRE}) = 0.5$ ,  $M_{\text{cr}} \sim 1.3 \times 10^{11} M_{\odot}$ , is also high with respect to optical studies.

*Consequences for selection of passive spirals.*—There exist spiral galaxies in our sample with undetected [O II] emission but significant MIR excess emission ( $^{0.4}[f(8)/f(3.6)] > 0.5$ ). Thus, selection of passive spirals based on a simple EW[O II] division (e.g., Poggianti et al. 1999; Balogh et al. 2002; Moran et al. 2006) will suffer contamination by dusty, low-level star formation, mostly early-type spirals.

*Strong suppression of activity for massive galaxies in low-mass groups.*—In the  $z \sim 0.4$  optically selected group environment there is a strong and robust ( $2.5 \sigma$ ) deficit in  $f(\text{IRE})$  compared with global values, *independent of stellar mass*. This is true across our range in stellar mass  $M_* \geq 2 \times 10^{10} M_{\odot}$ , but the suppression appears to be particularly strong at high mass,  $M_* \geq 10^{11} M_{\odot}$ , where the fraction of active group galaxies falls to  $f(\text{IRE}) = 0.12 \pm 0.07$ .

*Suppression in groups can drive the stellar mass dependence, and structure growth can drive downsizing.*—The global dependence of  $f(\text{IRE})$  on stellar mass at  $z = 0.4$  can be accurately reproduced by a simple model in which suppression mainly occurs in groups, and it is particularly strong for  $M_* \geq 10^{11} M_{\odot}$  group galaxies. Furthermore, structure growth in the universe drives more galaxies into group-sized halos with cosmic time. This automatically leads to a *downsizing* phenomenon in the global population, in which the crossover mass  $M_{\text{cr}}$  evolves to lower masses at lower redshift.

We thank the anonymous referee for substantial help with improving the manuscript. We would like to thank the CNOC2 team for allowing us access to their unpublished data and Eckhard Sturm for providing us with the calibrated ISO-SWS spectrum

of M82 in ASCII format. This work is based on observations made with the *Spitzer Space Telescope*, which is operated by the Jet Propulsion Laboratory, California Institute of Technology, under a contract with NASA. It is also based on observations made with the NASA/ESA *Hubble Space Telescope*, at the Space

Telescope Science Institute, which is operated by the Association of Universities for Research in Astronomy, Inc., under NASA contract NAS 5-26555. These observations are associated with program 9895. D. W. and D. P. are supported by the Max Planck Society.

## REFERENCES

- Aaronson, M., Huchra, J., & Mould, J. 1979, *ApJ*, 229, 1
- Aitken, D. K., Roche, P. F., Allen, M. C., & Phillips, M. M. 1982, *MNRAS*, 199, 31P
- Baldry, I. K., Balogh, M. L., Bower, R. G., Glazebrook, K., Nichol, R. C., Bamford, S. P., & Budavari, T. 2006, *MNRAS*, 373, 469
- Balogh, M., Bower, R. G., Smail, I., Ziegler, B. L., Davies, R. L., Gaztelu, A., & Fritz, A. 2002, *MNRAS*, 337, 256
- Balogh, M. L., et al. 2004, *MNRAS*, 348, 1355
- . 2007, *MNRAS*, 374, 1169
- Bell, E. F., & de Jong, R. S. 2001, *ApJ*, 550, 212
- Bell, E. F., et al. 2005, *ApJ*, 625, 23
- Bender, R., Saglia, R. P., Ziegler, B., Belloni, P., Greggio, L., Hopp, U., & Bruzual, G. 1998, *ApJ*, 493, 529
- Benson, A. J., Ellis, R. S., & Menanteau, F. 2002, *MNRAS*, 336, 564
- Berta, S., et al. 2007, *A&A*, 467, 565
- Bertin, E., & Arnouts, S. 1996, *A&AS*, 117, 393
- Best, P. N., von der Linden, A., Kauffmann, G., Heckman, T. M., & Kaiser, C. R. 2007, *MNRAS*, 379, 894
- Blanton, M. R., & Roweis, S. 2007, *AJ*, 133, 734
- Boselli, A., Lequeux, J., & Gavazzi, G. 2004, *A&A*, 428, 409
- Boselli, A., Sauvage, M., Lequeux, J., Donati, A., & Gavazzi, G. 2003, *A&A*, 406, 867
- Boselli, A., et al. 1998, *A&A*, 335, 53
- Bower, R. G., Benson, A. J., Malbon, R., Helly, J. C., Frenk, C. S., Baugh, C. M., Cole, S., & Lacey, C. G. 2006, *MNRAS*, 370, 645
- Bower, R. G., Lucey, J. R., & Ellis, R. S. 1992, *MNRAS*, 254, 601
- Bressan, A., et al. 2007, in *ASP Conf. Ser. 374, Early-Type Galaxies in the Mid-Infrared*, ed. A. Vallenari et al. (San Francisco: ASP), 333
- Brinchmann, J., Charlot, S., White, S. D. M., Tremonti, C., Kauffmann, G., Heckman, T., & Brinkmann, J. 2004, *MNRAS*, 351, 1151
- Bruzual, G., & Charlot, S. 2003, *MNRAS*, 344, 1000
- Bundy, K., et al. 2006, *ApJ*, 651, 120 (B06)
- Calura, F., Pipino, A., & Matteucci, F. 2008, *A&A*, 479, 669
- Calzetti, D., et al. 2007, *ApJ*, 666, 870
- Caputi, K. I., Dole, H., Lagache, G., McLure, R. J., Dunlop, J. S., Puget, J.-L., Le Floc'h, E., & Pérez-González, P. G. 2006, *A&A*, 454, 143
- Carlberg, R. G., Yee, H. K. C., Morris, S. L., Lin, H., Hall, P. B., Patton, D. R., Sawicki, M., & Shepherd, C. W. 2001, *ApJ*, 552, 427
- Chabrier, G. 2003, *PASP*, 115, 763
- Cimatti, A., et al. 2002, *A&A*, 381, L68
- . 2004, *Nature*, 430, 184
- Cowie, L. L., Songaila, A., & Barger, A. J. 1999, *AJ*, 118, 603
- Croton, D. J., et al. 2006, *MNRAS*, 365, 11
- Daddi, E., et al. 2007, *ApJ*, 670, 156
- Dale, D. A., et al. 2000, *AJ*, 120, 583
- Davoodi, P., et al. 2006, *MNRAS*, 371, 1113
- De Lucia, G., Springel, V., White, S. D. M., Croton, D., & Kauffmann, G. 2006, *MNRAS*, 366, 499
- Dekel, A., & Birnboim, Y. 2006, *MNRAS*, 368, 2
- Desert, F.-X., Boulanger, F., & Puget, J. L. 1990, *A&A*, 237, 215
- Draine, B. T., et al. 2007, *ApJ*, 663, 866
- Duc, P.-A., et al. 2002, *A&A*, 382, 60
- Eggen, O. J., Lynden-Bell, D., & Sandage, A. R. 1962, *ApJ*, 136, 748
- Engelbracht, C. W., Gordon, K. D., Rieke, G. H., Werner, M. W., Dale, D. A., & Latter, W. B. 2005, *ApJ*, 628, L29
- Fazio, G. G., et al. 2004, *ApJS*, 154, 10
- Fioc, M., & Rocca-Volmerange, B. 1997, *A&A*, 326, 950
- Fisher, D. B. 2006, *ApJ*, 642, L17
- Förster Schreiber, N. M., Genzel, R., Lutz, D., Kunze, D., & Sternberg, A. 2001, *ApJ*, 552, 544
- Förster Schreiber, N. M., Roussel, H., Sauvage, M., & Charmandaris, V. 2004, *A&A*, 419, 501
- Genzel, R., & Cesarsky, C. J. 2000, *ARA&A*, 38, 761
- Genzel, R., et al. 1998, *ApJ*, 498, 579
- Gerke, B. F., et al. 2007, *MNRAS*, 376, 1425
- Giovanelli, R., Haynes, M. P., Salzer, J. J., Wegner, G., da Costa, L. N., & Freudling, W. 1995, *AJ*, 110, 1059
- Gómez, P. L., et al. 2003, *ApJ*, 584, 210
- Gunn, J. E., & Gott, J. R. I. 1972, *ApJ*, 176, 1
- Haines, C. P., Gargiulo, A., & Merluzzi, P. 2008, *MNRAS*, 385, 1201
- Hammer, F., Flores, H., Elbaz, D., Zheng, X. Z., Liang, Y. C., & Cesarsky, C. 2005, *A&A*, 430, 115
- Hopkins, A. M. 2004, *ApJ*, 615, 209
- Hopkins, P. F., Bundy, K., Hernquist, L., & Ellis, R. S. 2007, *ApJ*, 659, 976
- Huang, J.-S., et al. 2007, *ApJ*, 664, 840
- Johnson, K. E., Hibbard, J. E., Gallagher, S. C., Charlton, J. C., Hornschemeier, A. E., Jarrett, T. H., & Reines, A. E. 2007, *AJ*, 134, 1522
- Kauffmann, G., et al. 2003, *MNRAS*, 341, 54
- Laurent, O., Mirabel, I. F., Charmandaris, V., Gallais, P., Madden, S. C., Sauvage, M., Vigroux, L., & Cesarsky, C. 2000, *A&A*, 359, 887
- Le Floc'h, E., et al. 2005, *ApJ*, 632, 169
- Leger, A., & Puget, J. L. 1984, *A&A*, 137, L5
- Lewis, I., et al. 2002, *MNRAS*, 334, 673
- Li, H.-N., Wu, H., Cao, C., & Zhu, Y.-N. 2007, *AJ*, 134, 1315
- Li, Y.-S., & White, S. D. M. 2008, *MNRAS*, 384, 1459
- Lilly, S. J., Le Fevre, O., Hammer, F., & Crampton, D. 1996, *ApJ*, 460, L1
- Lotz, J. M., et al. 2008, *ApJ*, 672, 177
- Madau, P., Pozzetti, L., & Dickinson, M. 1998, *ApJ*, 498, 106
- Masters, K. L., Giovanelli, R., & Haynes, M. P. 2003, *AJ*, 126, 158
- McGee, S. L., Balogh, M. L., Henderson, R. D. E., Wilman, D. J., Bower, R. G., Mulchaey, J. S., & Oemler, A., Jr. 2008, *MNRAS*, in press, (arXiv:0804.2693)
- Moran, S. M., Ellis, R. S., Treu, T., Salim, S., Rich, R. M., Smith, G. P., & Kneib, J.-P. 2006, *ApJ*, 641, L97
- Moran, S. M., Ellis, R. S., Treu, T., Smith, G. P., Rich, R. M., & Smail, I. 2007, *ApJ*, 671, 1503
- Pahre, M. A., Ashby, M. L. N., Fazio, G. G., & Willner, S. P. 2004a, *ApJS*, 154, 235
- . 2004b, *ApJS*, 154, 229
- Pannella, M., Hopp, U., Saglia, R. P., Bender, R., Drory, N., Salvato, M., Gabasch, A., & Feulner, G. 2006, *ApJ*, 639, L1
- Panter, B., Heavens, A. F., & Jimenez, R. 2003, *MNRAS*, 343, 1145
- Papovich, C., et al. 2006, *ApJ*, 640, 92
- Peeters, E., Spoon, H. W. W., & Tielens, A. G. G. M. 2004, *ApJ*, 613, 986
- Pérez-González, P. G., et al. 2006, *ApJ*, 648, 987
- Phillips, M. M., Aitken, D. K., & Roche, P. F. 1984, *MNRAS*, 207, 25
- Pierini, D., Maraston, C., Bender, R., & Witt, A. N. 2004, *MNRAS*, 347, 1
- Piovani, L., Tantaló, R., & Chiosi, C. 2003, *A&A*, 408, 559
- Poggianti, B. M., Bridges, T. J., Komiyama, Y., Yagi, M., Carter, D., Mobasher, B., Okamura, S., & Kashikawa, N. 2004, *ApJ*, 601, 197
- Poggianti, B. M., Smail, I., Dressler, A., Couch, W. J., Barger, A. J., Butcher, H., Ellis, R. S., & Oemler, A. J. 1999, *ApJ*, 518, 576
- Popescu, C. C., Misiriotis, A., Kylafis, N. D., Tuffs, R. J., & Fischera, J. 2000, *A&A*, 362, 138
- Postman, M., & Geller, M. J. 1984, *ApJ*, 281, 95
- Quilis, V., Moore, B., & Bower, R. 2000, *Science*, 288, 1617
- Rieke, G. H., et al. 2004, *ApJS*, 154, 25
- Rix, H.-W., & Rieke, M. J. 1993, *ApJ*, 418, 123
- Roche, P. F., Aitken, D. K., Smith, C. H., & Ward, M. J. 1991, *MNRAS*, 248, 606
- Roche, P. F., Whitmore, B., Aitken, D. K., & Phillips, M. M. 1984, *MNRAS*, 207, 35
- Roussel, H., Sauvage, M., Vigroux, L., & Bosma, A. 2001, *A&A*, 372, 427
- Rowan-Robinson, M., et al. 2005, *AJ*, 129, 1183
- Salim, S., et al. 2005, *ApJ*, 619, L39
- Salpeter, E. E. 1955, *ApJ*, 121, 161
- Shi, Y., et al. 2007, *ApJ*, 669, 841
- Springel, V., et al. 2005, *Nature*, 435, 629
- Tem, P., Brighenti, F., & Mathews, W. G. 2008, *ApJ*, 672, 244
- Thomas, D., Maraston, C., Bender, R., & Mendes de Oliveira, C. 2005, *ApJ*, 621, 673
- Tuffs, R. J., Popescu, C. C., Völk, H. J., Kylafis, N. D., & Dopita, M. A. 2004, *A&A*, 419, 821
- Wang, B., & Heckman, T. M. 1996, *ApJ*, 457, 645
- Weiner, B. J., et al. 2007, *ApJ*, 660, L39
- Weinmann, S. M., van den Bosch, F. C., Yang, X., & Mo, H. J. 2006, *MNRAS*, 366, 2

- Wilman, D. J., Balogh, M. L., Bower, R. G., Mulchaey, J. S., Oemler, A.,  
Carlberg, R. G., Morris, S. L., & Whitaker, R. J. 2005, MNRAS, 358, 71
- Wolf, C., Gray, M. E., & Meisenheimer, K. 2005, A&A, 443, 435
- Yamada, T., et al. 2005, ApJ, 634, 861
- Yan, R., Newman, J. A., Faber, S. M., Konidaris, N., Koo, D., & Davis, M.  
2006, ApJ, 648, 281
- Yee, H. K. C., et al. 2000, ApJS, 129, 475
- Zabludoff, A. I., & Mulchaey, J. S. 1998, ApJ, 496, 39
- Zheng, X. Z., Dole, H., Bell, E. F., Le Flo'ch, E., Rieke, G. H., Rix, H.-W., &  
Schiminovich, D. 2007, ApJ, 670, 301